AGU PUBLICATIONS

JGR

Journal of Geophysical Research: Space Physics

RESEARCH ARTICLE
10.1002/2015JA021512

Special Section:
Big Storms of the Van Allen Probes Era

Simulation of low-latitude ionospheric response to 2015 St. Patrick's Day super geomagnetic storm using ionosonde-derived PRE vertical drifts over Indian region

L. M. Joshi[1], S. Sripathi[1], and Ram Singh[1]

[1]Indian Institute of Geomagnetism, New Bombay, India

Key Points:
- Coincidence of prompt penetration of electric field and PRE resulted in 60-70 m/s vertical drift
- Model indicated increase in F layer height in main phase and EIA suppression in recovery phase
- Model results have also been compared with ground GPS TEC observations

Correspondence to:
L. M. Joshi,
lmjoshinarl@gmail.com

Citation:
Joshi, L. M., S. Sripathi, and R. Singh (2016), Simulation of low-latitude ionospheric response to 2015 St. Patrick's Day super geomagnetic storm using ionosonde-derived PRE vertical drifts over Indian region, *J. Geophys. Res. Space Physics*, *121*, doi:10.1002/2015JA021512.

Received 29 MAY 2015
Accepted 6 FEB 2016
Accepted article online 26 FEB 2016

Abstract In this paper, we present low-latitude ionospheric response over Indian longitude to the recent super geomagnetic storm of 17 March 2015, using the Sami2 is Another Model of the Ionosphere (SAMI2) model which incorporates ionosonde-derived vertical drift impacted by prompt penetration eastward electric field occurring during the evening prereversal enhancement (PRE) in the vertical drift. The importance of this storm is that (1) *Dst* reaches as low as −228 nT and (2) prompt penetration of eastward electric field coincided with evening hours PRE. The daytime vertical E × B drifts in the SAMI2 model are, however, considered based on Scherliess-Fejer model. The simulations indicate a significant enhancement in *F* layer height and equatorial ionization anomaly (EIA) in the post sunset hours on 17 March 2015 vis-a-vis quiet day. The model simulations during recovery phase, considering disturbance dynamo vertical E × B drift along with equatorward disturbance wind, indicate suppression of the daytime EIA. SAMI2 simulations considering the disturbance wind during the recovery phase suggest that equatorward wind enhances the ionospheric density in the low latitude; however, its role in the formation of the EIA depends on the polarity of the zonal electric field. Comparison of model derived total electron content (TEC) with the TEC from ground GPS receivers indicates that model does reproduce enhancement of the EIA during the main phase and suppression of the EIA during the recovery phase of the superstorm. However, peculiarities pertaining to the ionospheric response to prompt penetration electric field in the Indian sector vis-a-vis earlier reports from American sector have been discussed.

1. Introduction

Ionospheric response to space weather events has been a subject of extensive scientific investigations [e.g., *Sastri*, 1988; *Fesen et al.*, 1989; *Abdu et al.*, 1998, 2012; *Fejer*, 1997; *Ho et al.*, 1998; *Jakowski et al.*, 1999; *Kikuchi et al.*, 2000; *Tsurutani et al.*, 2004, 2008; *Maruyama et al.*, 2004; *Foster and Rideout*, 2005; *Fejer et al.*, 2007; *Astafyeva*, 2009; *Galav et al.*, 2014; *Carter et al.*, 2014]. Over the low latitudes, such response becomes remarkable during major geomagnetic storms [e.g., *Abdu et al.*, 1998, 2012]. During storm periods, dynamical and electrodynamical changes are often observed in the low-latitude ionosphere. Such changes alter the latitudinal structure of the low-latitude ionosphere and causes total electron content (TEC) to change [e. g., *Rastogi and Klobuchar*, 1990; *Sharma et al.*, 2011; *Galav et al.*, 2011]. It can severely affect the performance of satellite-based navigation and communication systems. Thus, the ionospheric response of the geomagnetic storm needs to be modeled and forecasted in advance for unhindered navigation and communication applications.

Electrodynamical changes in the low-latitude ionosphere during the geomagnetically disturbed days can occur due to the prompt penetration (PP) of magnetospheric electric field and disturbance dynamo (DD) electric field, in addition to the changes brought about by the disturbed thermospheric winds in the recovery phase. The PP electric fields are quite transient in nature [e.g., *Gonzales et al.*, 1979; *Kikuchi et al.*, 1996, 2000] which penetrate to the low latitudes during sudden southward (undershielding electric field) or northward (overshielding electric field) turning of interplanetary magnetic field (IMF) marking the different phases of a geomagnetic storm [*Fejer and Scherliess*, 1997]. As the PP occurs during a sudden change in the IMF, it lasts for a short duration of ~30–90 min. The direction of the PP field is determined by the nature of the field itself. At magnetic equator the undershielding (overshielding) electric field is generally directed eastward (westward) during the day [*Kelley et al.*, 1979; *Fejer*, 2002], while in the night sector, the directions of the PP fields are opposite to that in the day sector. During a geomagnetic storm, Joule heating of the upper atmosphere over high latitudes often results in global variation of the thermospheric wind system that produces disturbance dynamo

electric field observed with nonuniform time delays at different latitudes [*Blanc and Richmond*, 1980]. Disturbance dynamo field could last for a few hours up to more than a day [*Richmond et al.*, 2003]. At the magnetic equator, the disturbance dynamo electric field is directed eastward (westward) at the night (day) sector [*Scherliess and Fejer*, 1997].

Geomagnetic storm that commenced on 17 March 2015 was the first superstorm of the solar cycle 24, where *Dst* has dropped to ~ −228 nT. Effects of this superstorm were observed in the *F* region vertical E × B drift recorded at Tirunelveli (8.5°N, 78.2°E, 0.5°N magnetic latitude), a station located at the magnetic equator in India, using the Doppler sounding with a Canadian Advanced Digital Ionosonde (CADI) [*Grant et al.*, 1995; *Abdu et al.*, 1998]. A detailed account of the observations corresponding to the 17 March 2015 superstorm has already been reported by *Singh et al.* [2015]. Current paper deals with the Sami2 is Another Model of the Ionosphere (SAMI2) modeling of the ionospheric distribution during the different phases of the superstorm. Vertical E × B drift measured using the Doppler sounding with CADI is used as input to the modified SAMI2 code [*Huba et al.*, 2000] to model the impact of PP and DD fields, associated with the superstorm, on the dynamical evolution of the ionosphere over Indian longitude. Evolution of the equatorial ionization anomaly (EIA) as obtained by the SAMI2 model during different phases of the geomagnetic storm is compared with the latitudinal variation of vertical TEC over Indian longitude derived from GPS receiver network. There have been various reports on the study and the modeling of the low-latitude ionospheric response to space weather events over different longitude sectors [e.g., *Batista et al.*, 1991; *Lin et al.*, 2005a, 2005b]. However, this manuscript presents the modeling of the low-latitude ionospheric redistribution during an intense geomagnetic storm, for the first time over Indian sector.

2. Observations, Data, Model, and Methodology

Interplanetary parameters discussed in the present work include the interplanetary magnetic field (B_z), solar wind speed (V_{sw}), and the interplanetary electric field (E_y). ACE satellite positioned at the L1 point between the Sun and the Earth enables continuous monitoring of the solar and interplanetary variables on a continuous basis. Interplanetary electric field, E_y is calculated as $E_y = -V_{sw}B_z$. These data sets are available through openly accessible data repository (http://cdaweb.gsfc.nasa.gov/). Disturbance storm time (*Dst*) index has been obtained from the world data center (WDC) Kyoto.

The *F* region vertical plasma drift is measured using a Canadian Advanced Digital Ionosonde (CADI) that was operated in its fixed frequency Doppler sounding mode, at 7 MHz, from Tirunelveli, a magnetic equatorial station in India. Doppler sounding with CADI is a well-established technique to derive the vertical plasma drift of the *F* layer [*Cannon et al.*, 1991; *Grant et al.*, 1995; *Abdu et al.*, 1998]. Receiving antenna array in the CADI system consists of four dipoles arranged along the sides of a square with length of 30 m. Each receiving dipole is attached to a separate receiver. Drift measurement is carried out at a rate of 0.016 Hz, i.e., 60 s for each measurement. For that, a 64 point complex time series is generated every 60 s for each range bin of all the four antennas. Data integration is also carried out to reduce its storage size. This 64 point time series is Fourier transformed in real time for all the range bins of each antenna to generate power spectra. Least squares fitting is carried out to the power spectrum to make it smooth. The range bin with maximum received power is identified for the first antenna and is set for all the four antennas. If this received power is above a certain noise threshold, then only the power spectrum can be utilized to derive the Doppler shift. Thus, there can be a data gap in the Doppler measurement if the received power is not sufficient. Frequency bin in the power spectrum with the maximum power in all four antennas represents the Doppler shift of the received signal. Line of sight drift is calculated by multiplying the Doppler shift with half of the operating wavelength, $\lambda/2$. Thus, the method of calculating the Doppler drift in CADI system is quite similar to the one employed in a coherent scatter radar (CSR), except for the operating frequency. A CSR usually operates in the VHF band, while CADI operates in the HFs in the range of 1–20 MHz. In the present case 7 MHz operating frequency has been utilized for the Doppler measurements. For more literature on the ionosonde Doppler technique, one can refer to *Bibl and Reinisch* [1978], *Grant et al.* [1995], *Cannon et al.* [1991], and the references therein. In the present case, along with the Doppler soundings, regular swept frequency sounding was also carried out once in every 10 min using the CADI, to derive standard ionosonde parameters like h'F and f_oF_2. While the ionosonde Doppler technique provides a fair estimation of the vertical E × B drift during the evening hours, it severely underestimates the E × B drift during the daytime. CADI measures the vertical drift based on the Doppler detection of the reflected

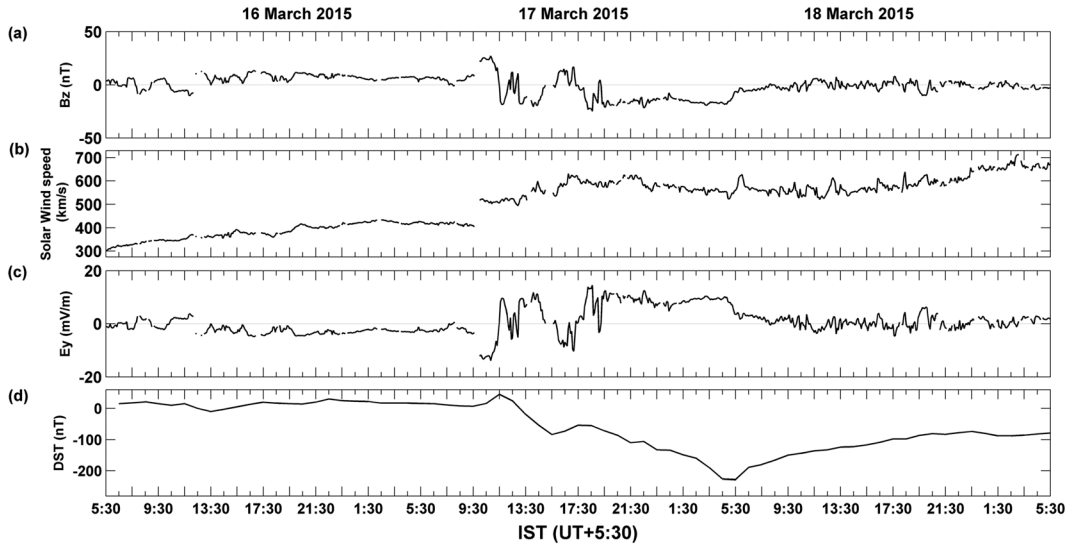

Figure 1. Interplanetary and geomagnetic conditions during 16–18 March 2015. (a) Variation of the *z* component (B_z) of interplanetary magnetic field in GSM coordinates. (b) The solar wind speed. (c) Interplanetary electric field (E_y) in mV/m. (d) *Dst* index (nT) on 16–18 March 2015.

echoes (unlike the scattered echoes and as in the case of CSR or incoherent scatter radar). The HF reflection occurs from an altitude where electron density value corresponds to the plasma frequency, i.e., the reflected frequency. The height of the isoelectron density surface (the reflection height) is determined by the electric field as well as the photochemistry (the ionization production and the recombination loss). Thus, the Doppler velocity determined from the changes in the *F* layer height is also subject to photochemistry during the daytime. As a result, the Doppler E × B drift in HF is a severe underestimation of the actual E × B drift during the daytime. Considering this limitation, for the present investigation, the CADI-measured vertical E × B drift has been only utilized in the post sunset period between 18 and 21 h, while the vertical E × B drift during the remaining hours of the day has been considered based on the Scherliess-Fejer E × B drift model [*Scherliess and Fejer*, 1997; *Scherliess and Fejer*, 1999].

Zonal electric field, causing vertical E × B plasma drift over the magnetic equator (vertical E × B drift) plays the dominant role in the transport and the distribution of the ionospheric plasma in the low latitudes. During the daytime it drives the equatorial fountain and generates the equatorial ionization anomaly, while in the post sunset periods it transports the *F* region plasma to a very high altitude. In the post sunset period, enhancement of the zonal electric field also leads to a resurgence of the EIA. In the present study, the vertical E × B drift based on the CADI measurements during the evening hours and model vertical E × B drift for the remaining period have been used as input into the SAMI2 model to understand the ionospheric redistribution over the Indian region during the intense magnetic storm. The vertical E × B drift considered in the model includes the disturbance dynamo component relevant during an intense magnetic storm. The SAMI2 is a versatile physics-based ionospheric model which simulates the chemical and dynamical evolution of seven major ionic species along the entire magnetic flux tube [*Huba et al.*, 2000]. SAMI2 model in its default form includes the vertical plasma drift from the E × B drift model [*Scherliess and Fejer*, 1999]. The default vertical drift model of the SAMI2 was replaced by the modified vertical drift relevant for the storm period. Also, disturbance meridional wind has been considered in the recovery phase of the storm, based on the literature and horizontal wind model (HWM) model, which is included in the SAMI2. These modifications are, however, minor in nature, as the aspects other than the vertical E × B drift and the disturbance neutral winds remains the same as in the default version of the SAMI2 code. Default version of the SAMI2 model considers the vertical E × B drift to be height independent, which has been retained as such in the present investigation (storm time vertical drift may be mostly height independent). Thus, an effort has been made to simulate the ionospheric response in terms of its altitudinal-latitudinal structure to the observed variations in the equatorial vertical E × B drift during the superstorm.

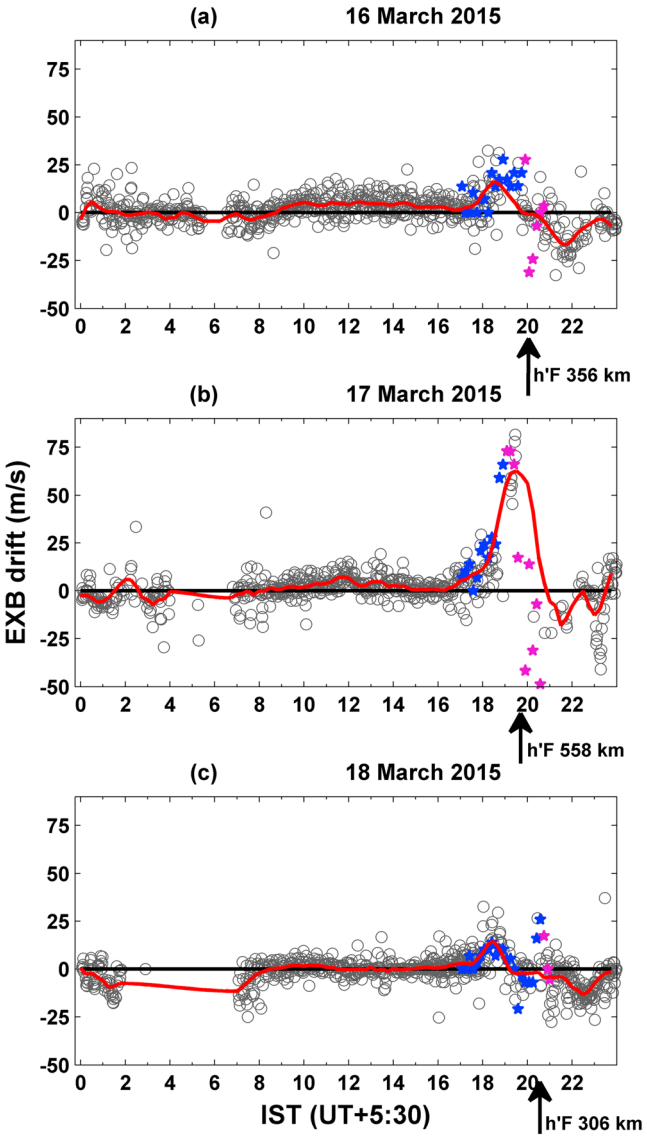

Figure 2. Vertical E × B drift recorded over Tirunelveli on (a) 16 March 2015, (b) 17 March 2015, and (c) 18 March 2015. Here each grey circle represents the Doppler E × B drift at a particular time; the red line represents the averaged, smoothed Doppler E × B drift. Blue and purple colored stars shown in the evening and post sunset period indicate the E × B drift derived by the rate of change of the *F* layer height ($V_z = dh'F/dt$); blue colored stars indicate the presence of clear *F* region trace, while purple color stars represent the spread *F* in the ionograms. Bold arrow below the time axis and the text adjacent to it indicate the peak h'F recorded by the CADI.

Total electron content (TEC) map has been generated, utilizing GPS TEC observations from six receiver stations (Tirunelveli, Bangalore, Hyderabad, Nagpur, Rajkot, and Lucknow) located over the Indian region, to observe the behavior of EIA during different phases of the geomagnetic storm.

3. Results and Discussion

3.1. IMF B_z Variations and *Dst* Index During Severe Geomagnetic Storm

The geomagnetic storm that occurred on 17 March 2015 is the first severe geomagnetic storm of the current solar cycle 24, with the *Dst* index dropping to −228 nT. Two coronal mass ejections (CME) occurred on 15 March that traveled in the interplanetary space as halo CMEs and hit the earth on 17 March causing a major geomagnetic storm. Figures 1a–1d shows the IMF B_z, the solar wind speed, the interplanetary electric field E_y, and the *Dst* index on 16–18 March 2015. The southward turning of the IMF B_z began ~12:00 IST (Indian standard time, UT + 5:30) on 17 March. This was preceded by an abrupt increase in the solar wind speed, indicating the halo CME hitting the Earth's magnetosphere. The interplanetary electric field shown in the Figure 1c also shows a similar behavior with its sudden eastward turning. Looking at the *Dst* index, the decrease in the *Dst* began at around 12:00 IST on 17 March that was preceded by the southward turning of the IMF B_z. A partial/short-lived recovery in the *Dst* can be seen around 16:00 IST on 17 March. This break in the reduction of *Dst* was preceded by the northward turning of the IMF B_z. The IMF B_z again displayed the southward turning at around 17:30 IST on 17 March, which resulted in the main phase of the geomagnetic storm with continuous reduction in the *Dst* index. Beyond this, except for the fluctuations, IMF B_z remained southward till 05:30 IST on 18 March. The two-step reduction in the *Dst* value gives a clear signature of the two CMEs that occurred on 15 March. *Dst* index was recorded minimum at −228 nT at 05:30 IST on 18 March. This was followed by the recovery of the storm.

3.2. Doppler Vertical Drifts Over Tirunelveli During Different Phases of the Superstorm

CADI, installed at Tirunelveli, has been operated in the Doppler mode to measure the vertical E × B drift in the *F* region over the magnetic equator in the Indian sector. Figures 2a–2c show the vertical E × B drift recorded by CADI on 16–18 March, respectively. Here each grey circle represents, the Doppler E × B drift recorded at a

particular time. Thick red line represents the averaged, smoothened Doppler E × B drift. In the evening and the post sunset hours, it is also possible to calculate the *F* layer vertical drift by monitoring the rate of change of the *F* layer height. Blue and purple stars shown for the evening and the post sunset hours in Figure 2 show the *F* layer vertical drift velocities, calculated by monitoring the *F* layer height rise $V_z = dh'F/dt$. Here blue color star indicates the presence of clear *F* layer trace, while the purple star indicates the spread *F* period. It is interesting to see that the *F* region vertical drift calculated using Doppler detection is in a good agreement with the drift values calculated by monitoring the *F* layer height.

Although the broad features of the vertical E × B drift shown in Figure 2 in terms of its direction are in accordance with the known facts, however, its amplitude during the daytime is too small to be realistic. As mentioned earlier, the Doppler E × B drift measured in the HFs during the daytime is an underestimation of the actual vertical drifts due to the photochemistry that controls the height [*Bertoni et al.*, 2006]. However, during the evening and post sunset hours the Doppler E × B drifts measured in the HF band provides a reasonable estimation of the actual vertical E × B drift [*Bertoni et al.*, 2006; *Woodman et al.*, 2006]. It can be noted that on 17 March, during the evening hours, close to the time of the prereversal enhancement, vertical E × B drift displayed a very large enhancement with peak E × B drift in the range of 60–70 m/s. However, such large prereversal enhancement of the zonal field was not observed on 16 and 18 March. The Interplanetary electric field also turned eastward at prereversal enhancement (PRE) time on 17 March (refer to Figure 1c), which indicates that the enhanced *F* region drift was an outcome of the prompt penetration of the magnetospheric electric field. The peak *F* layer drift in the range of 60–70 m/s on 17 March was more than double its value on 16 and 18 March. In the Indian region, the peak *F* layer vertical drift during the post sunset hours in the equinox period of moderate to high solar activity conditions usually remains in the range of 15–30 m/s. Thus, the intense vertical E × B drift in the post sunset hours on 17 March is much higher than the usual values.

In Figure 2, bold arrows marked under the time axis and text along it indicates the peak h′F recorded by the CADI. It can be noted that the peak h′F was 558 km on 17 March, which is 200 km more than that on 16 March. Peak h′F in the range of 360–420 km over magnetic equator in the Indian sector during geomagnetically quiet days represents a very high degree of post sunset height rise [*Joshi et al.*, 2015]. Thus, the intense increase in the E × B drift after 17:30 IST on 17 March and the associated rise of the *F* layer were a direct outcome of the penetration of the high-latitude electric field on the equatorial region. *Sobral et al.* [1997] have earlier reported intense enhancement to the *F* layer height over Fortaliza, Brazil, in the evening hours due to the prompt penetration of the magnetospheric electric field. Owing to the inherent limitation of the HF Doppler sounding during the daytime, the effect of the disturbance dynamo electric field cannot be substantiated during the recovery phase using the ionosonde measurement. The vertical drift during the daytime has been ascertained based on the E × B drift model, namely, Scherliess-Fejer (SF) model.

3.3. Vertical E × B Drifts Used as Input in the SAMI2 Simulations

While the feature of the PP field could be recorded in the ionosonde Doppler, reliable vertical E × B drift value during the recovery phase owing to the DD field could not be derived. Unlike the PP field, the DD field is nontransient in nature and sets in with a delay of more than a few hours of the geomagnetic disturbance. The strongest part of the DD field over the magnetic equator usually appears in the recovery phase of the geomagnetic storm, with a delay of more than 16–20 h after the onset of storm [*Blanc and Richmond*, 1980; *Sastri*, 1988; *Scherliess and Fejer*, 1997].

The ionospheric disturbance dynamo is being discussed briefly here. Field-aligned currents during the active phases of the magnetic storm enhance the auroral electrojet strength. Joule heating associated with the enhanced auroral electrojet transfers the thermal energy to the neutral atmosphere. This leads to the equatorward flow of the neutral wind and Hadley cell between the equator and the poles. Equatorward winds flow from poles to the low latitude at altitudes above 120 km. A return flow from equator to the poles takes place above the *E* region altitude between 110 and 120 km [*Blanc and Richmond*, 1980]. Due to the Coriolis turning by the action of the Earth's rotation, equatorward meridional flow drives a westward zonal flow. Dynamo action associated with the westward winds and the vertical component of the Earth's magnetic field gives rise to equatorward Pedersen current. This in turn generates a poleward electric field. Poleward field produces a westward plasma flow and an eastward Hall current. Eastward Hall currents produce a westward polarization electric field. This whole process has been termed as the ionospheric disturbance dynamo by *Blanc and Richmond* [1980].

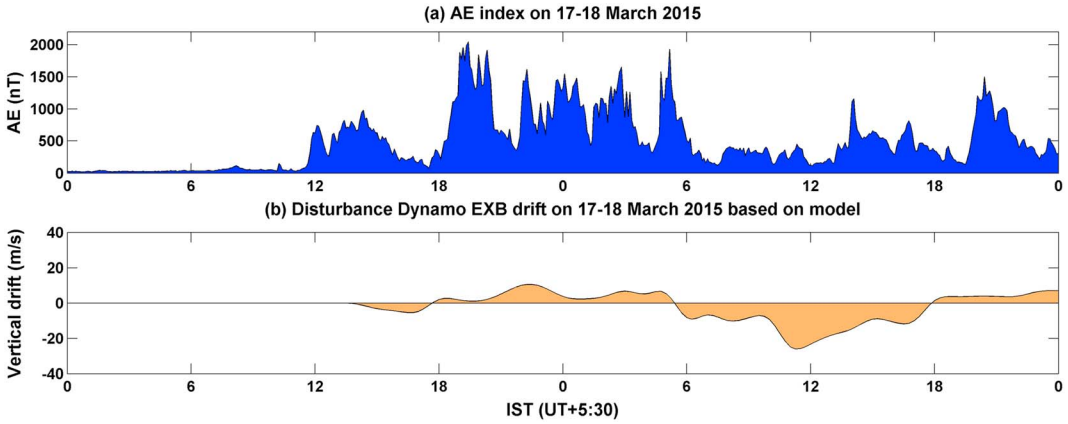

Figure 3. (a) Auroral electrojet index during the 17–18 March 2015. (b) Disturbance dynamo electric field calculated using the Scherliess and Fejer model [*Scherliess and Fejer*, 1997].

Auroral electrojet (*AE*) index is considered to be proportional to the enhanced energy deposition in the thermosphere. *Scherliess and Fejer* [1997], based on two decades of the Jicamarca vertical E × B drift, derived an empirical relation between the time series of the *AE* index and the disturbance dynamo vertical E × B drift. Empirical model calculates the short-term and long-term components of the disturbance dynamo vertical E × B drift utilizing the time series of the *AE* index. In the present investigation, the empirical model has been utilized to derive the disturbance dynamo vertical E × B drift over the equator. Figures 3a and 3b show the *AE* index and the model disturbance vertical E × B drift, respectively, during 17–18 March 2015. Here moderate disturbance dynamo E × B drift can be seen a few hours after the onset of the magnetic storm; however, the maximum magnitude of the disturbance dynamo E × B drift can be seen during the recovery phase ~12 IST on 18 March. This disturbance dynamo E × B drift has been added to the quiet period vertical E × B drift to derive the net vertical E × B drift. However, vertical E × B drift during the post sunset period, i.e., 18–21 IST, on 16–18 March has been considered based on the ionosonde Doppler measurement. The vertical E × B drift utilized in the SAMI2 model is being presented next.

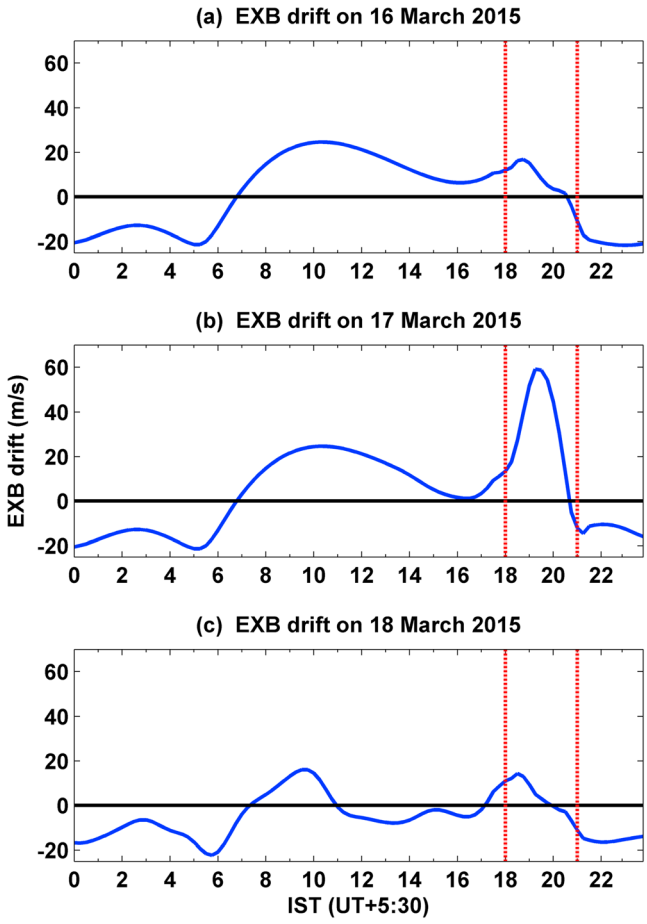

Figure 4. Vertical E × B drift utilized in the SAMI2 model for (a) 16 March 2015, (b) 17 March 2015, (c) and 18 March 2015.

Figure 4 shows the vertical E × B drift during 16–18 March 2015, which has been used as inputs in the SAMI2 model. Here Figures 4a–4c present the vertical E × B drift on 16–18 March 2015, respectively. Here vertical E × B drift values on 16–18 March during 18–21 IST periods, as marked by dashed red vertical lines, has been considered based on the Doppler measurement presented in

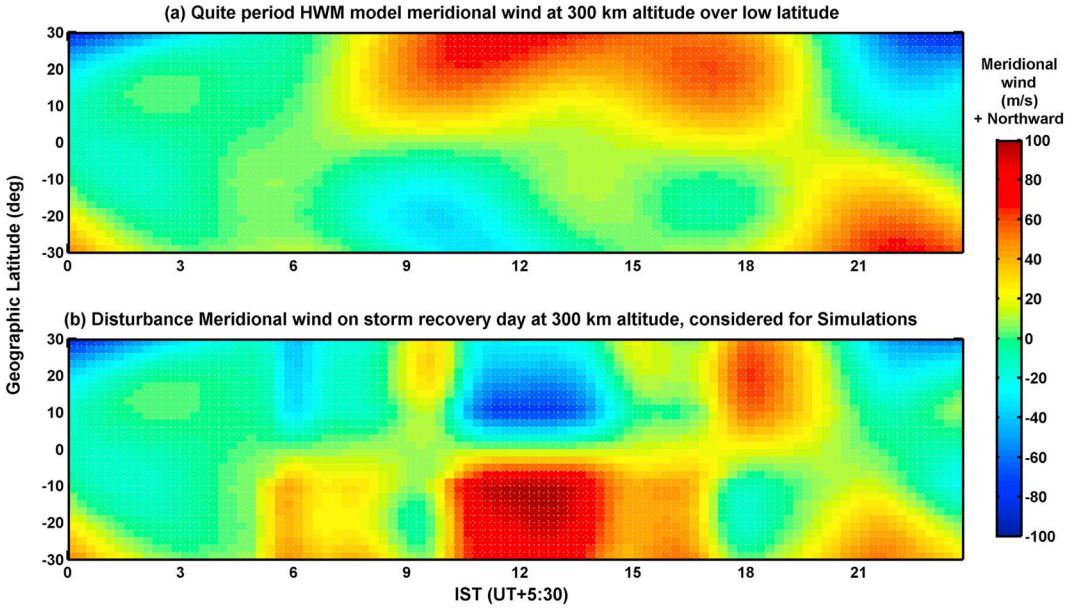

Figure 5. (a) Quiet period meridional wind based on the HWM model. (b) Disturbance meridional wind considered in the SAMI2 model during the recovery phase of the geomagnetic storm on 18 March 2015.

Figure 2 earlier. In Figure 4 the vertical E × B drift during the daytime and after the PRE hours have been considered based on the SF model. The vertical E × B drift on 16 March 2015 represents the quiet time drift, whereas the vertical E × B drift on 17 and 18 March 2015 includes the disturbance E × B drift forcing on the quiet time value. Notable features here are large upward drift during the post sunset period on 17 March due to the prompt penetration of the electric field and downward drift during the daytime on 18 March due to the ionospheric disturbance dynamo. Also, it shows near zero vertical E × B drift in the 16–17 IST on 17 March. Reversal of the E × B drift during the daytime in the recovery phase of the geomagnetic storm has been previously reported in several earlier investigations [e.g., *Fejer et al.*, 1983; *Scherliess and Fejer*, 1997; *Abdu et al.*, 2006]. The daytime vertical plasma drift in the recovery phase can be downward if the disturbance westward electric field exceeds the quiet time eastward electric field. Although suppression of PRE drift is known to occur during the storm recovery phase, however, in Figure 4c, one does not see such a behavior. Vertical E × B drift shown in Figure 4 has been used as input to the SAMI2 model to study the low-latitude ionospheric response to different phases of geomagnetic storm.

Not only the disturbance dynamo electric field produces the anomalies in the low-latitude ionospheric evolution during the recovery phase but also the disturbance meridional neutral winds plays an important role in modifying the ionospheric density and its latitudinal structure. Thus, in the model simulations, disturbance neutral winds have also been considered to be active during the recovery phase of the geomagnetic storm. The disturbance meridional wind during the recovery phase will be discussed next.

3.4. Storm Time Meridional Winds During the Recovery Phase

Although the primary driver of the EIA is the zonal electric field, meridional neutral wind contributes significantly to the low-latitude plasma densities. Equatorward wind pushes the ions upward along the magnetic field line and enhances the electron density over the magnetic equator. Joule heating in the auroral region changes the entire pattern of the neutral winds. Although the changes in the neutral winds during the recovery phase of the geomagnetic storm are most pronounced in the high latitudes, its significance in the low latitude remains high. Investigations in the past have reported equatorward disturbance wind surge of 300 m/s over high latitudes and 100 m/s over the low latitudes. Recently, *Haaser et al.* [2013] reported the equatorward wind surges in the low latitudes that appeared after the recovery of the storm commenced and lasted for several hours. Based on a case study comprising five magnetic storms, they have found the equatorward wind surges in the low latitude with winds in the range of 70–100 m/s lasting for 5–12 h. Thus, such meridional wind surges have been assumed for model computations in the present investigation. Figures 5a and 5b show the

meridional wind at 300 km during the quiet period and during the disturbed period, respectively, considered for the model computations. Here Figure 5a presents the quiet period meridional wind based on the HWM model. HWM model is a constituent of the SAMI2 ionospheric model. It can be noted that the quiet period meridional wind is poleward during the daytime. Thus, HWM model fails to indicate equatorward disturbance wind surges during the recovery phase of the geomagnetic storm. For this reason, equatorword wind perturbations have been introduced in the HWM model winds. Figure 5b indicates the meridional neutral wind considered for the model computation for 18 March 2015, i.e., during the recovery phase. The meridional wind for 18 March has been constructed by adding 120 m/s equatorward wind surges to the quiet period wind normalized with the DD field shown in the Figure 3. This means that the equatorward wind surge has been considered to be 120 m/s at the time of maximum magnitude of the DD electric field, while at other times the equatorward wind surges have been normalized with respect to the maximum DD field. As mentioned earlier, *Haaser et al.* [2013] reported the disturbance wind surges to be in the range of 70–100 m/s. Their study was based on five geomagnetic storms, in which the maximum drop in the *Dst* was in the range of 90 to 180 nT. Geomagnetic storm under consideration in the present investigation has a drop in the *Dst* of ~228 nT. Thus, the peak amplitude of disturbance equatorward wind surge in the present case has been considered somewhat higher, i.e., 120 m/s. Also, the equatorward wind has been assumed to gradually start reducing after 10° latitude and become 0 at the equator. Thus, the interhemispheric disturbance winds have not been considered in the present investigation, for simplicity. However, theoretical investigations in the past have indicated the formation of additional ionization layer in the EIA owing to the interhemispheric disturbance winds [*Lin et al.*, 2009]. Disturbance meridional wind indicated in Figure 5 has been constructed based on the method mentioned above. Such a methodology has been adopted in the absence of any systematic observation of thermospheric neutral wind in the Indian sector, particularly during the daytime.

3.5. SAMI2-Based Modeling Results

SAMI2 model is a versatile physics-based low- to middle-latitude model that simulates the dynamical and chemical evolution of the ionosphere [*Huba et al.*, 2000]. In its default form it assumes the magnetic field perpendicular vertical E × B drift of the ionosphere either to be sinusoidal or to be defined by the E × B drift model [*Scherliess and Fejer*, 1999]. Zonal electric field is the most important driver of the EIA. Thus, for the present study the default vertical E × B drift in the SAMI2 has been replaced by a combination of the vertical E × B drift based on model and CADI observations. The vertical E × B drift shown in Figure 4 has been utilized as input to the SAMI2 model. Thus, the model output is expected to figure out the effect of the geomagnetic storm on the low-latitude ionosphere.

Figure 6 shows the evolution of the EIA in the low-latitude ionosphere in the SAMI2 model for 16 March 2015. It represents the quiet day low-latitude ionosphere over the Indian longitude. Here Figures 6a–6d indicate the latitudinal-altitudinal structure of the low-latitude ionosphere over the Indian region at 14, 16, 18, and 20 IST, respectively. *X* axis shows the geographic latitude, with geomagnetic latitude indicated in parentheses. EIA formation can be seen during the daytime. Trough of the EIA is seen at magnetic equator, while the crest is located at around 12°–15° magnetic latitude. Also, the height rise of the *F* layer in the vicinity of the magnetic equator due to the PRE of the zonal field can be seen at 20:00 IST. However, this height rise is quite moderate owing to the moderate E × B vertical drift during post sunset hours on 16 March (as seen in Figure 4).

Evolution of the EIA in the SAMI2 model for 17 March 2015 is shown in Figure 7. Well-defined EIA crest/trough region can be seen. The most notable deviation from the quiet period ionosphere is the large post sunset height rise. In Figure 7d the height of the *F* layer over magnetic equator at 20:00 IST is much higher than that in Figure 6d. It represents the effect of the prompt penetration electric field during the evening hours on 17 March 2015. As indicated in Figure 2 earlier, the peak h'F was significantly higher on 17 March in comparison with that on 16 March. Thus, the higher *F* layer height owing to the large prereversal E × B drift can be seen in the SAMI2 model results as well. Height rise of the *F* layer in Figure 7d is seen only in the vicinity of the magnetic equator, and such height rise is not seen over the EIA crest latitudes. Due to the inclined magnetic field lines in the low latitudes, only a component of the E × B drift is projected in the upward direction. Also, plasma from higher altitudes diffuses along the magnetic field lines to lower altitudes, which prevents the *F* layer to rise significantly in the EIA crest region. However, large E × B drift can also cause a significant latitudinal expansion of the EIA

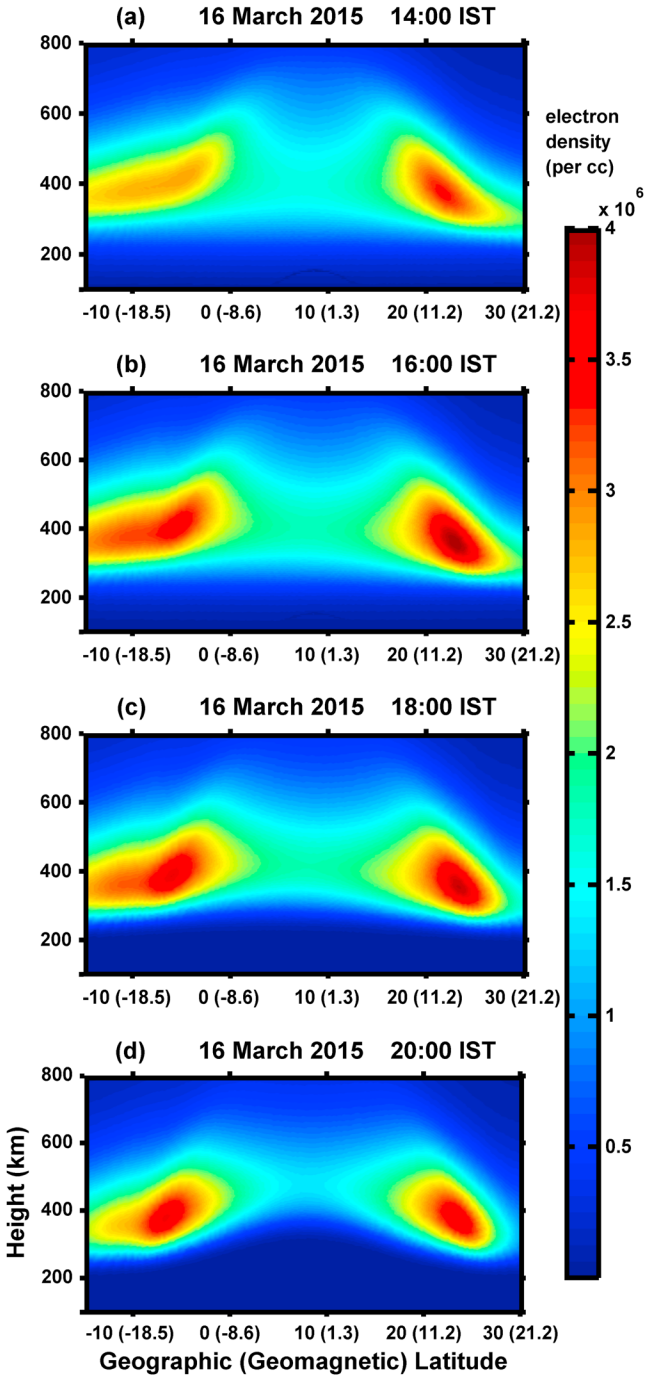

Figure 6. Latitudinal-Altitudinal distribution of the ionospheric plasma over Indian longitude in the SAMI2 model on 16 March 2015 (quiet period) at (a) 14 IST, (b) 16 IST, (c) 18 IST, and (d) 20 IST.

crest, through enhanced fountain effect. The plasma density over the magnetic equator (low latitude) at 20:00 IST on 17 March was less (more) than that on 16 March (as can be seen in Figures 6 and 7). This is a possible outcome of the super fountain effect associated with the prompt penetration electric field.

The daytime ionospheric behavior on 18 March 2015 can be expected to differ significantly from the quiet period ionosphere due to the influence of the DD field and the disturbance meridional wind. The low-latitude ionosphere in the SAMI2 model on 18 March 2015 will be discussed next. Figure 8 shows the latitudinal-altitudinal structure of the low-latitude ionosphere in the SAMI2 model for 18 March 2015. Here Figures 8a–8d present the SAMI2 model ionosphere for 18 March 2015, considering the disturbance vertical $E \times B$ drift and quiet period meridional wind. Whereas, Figures 8e–8h present the same, but considering the disturbance meridional wind, in place of quiet period meridional wind. Thus, the model computation can be expected to reveal the respective role of the DD field and the disturbance neutral wind during the recovery phase of the superstorm. Two of the important aspects presented here are the following: (1) there is a remarkable suppression of the EIA on 18 March and (2) the disturbance meridional wind enhances the plasma density in the equatorial and low latitudes. Coming to the EIA, it seems evident that the eastward electric field is a necessary condition for the well-defined EIA crest/trough to exist. Enhancement of the plasma density over the equatorial and low latitudes, when equatorward disturbance winds are considered in model, is in accordance with the previously reported results [*Balan et al.*, 2013; *Lin et al.,* 2005a, 2005b]. *Balan et al.* [2013] have reported that the equatorward neutral wind during the recovery phase of the magnetic storm, even in the presence of westward disturbance dynamo electric field, enhances the plasma density over the magnetic equator. Equatorward neutral wind pushes the ionospheric plasma upward along the magnetic field line and toward the magnetic equator. However, the absence of well-defined EIA on 18 March suggests

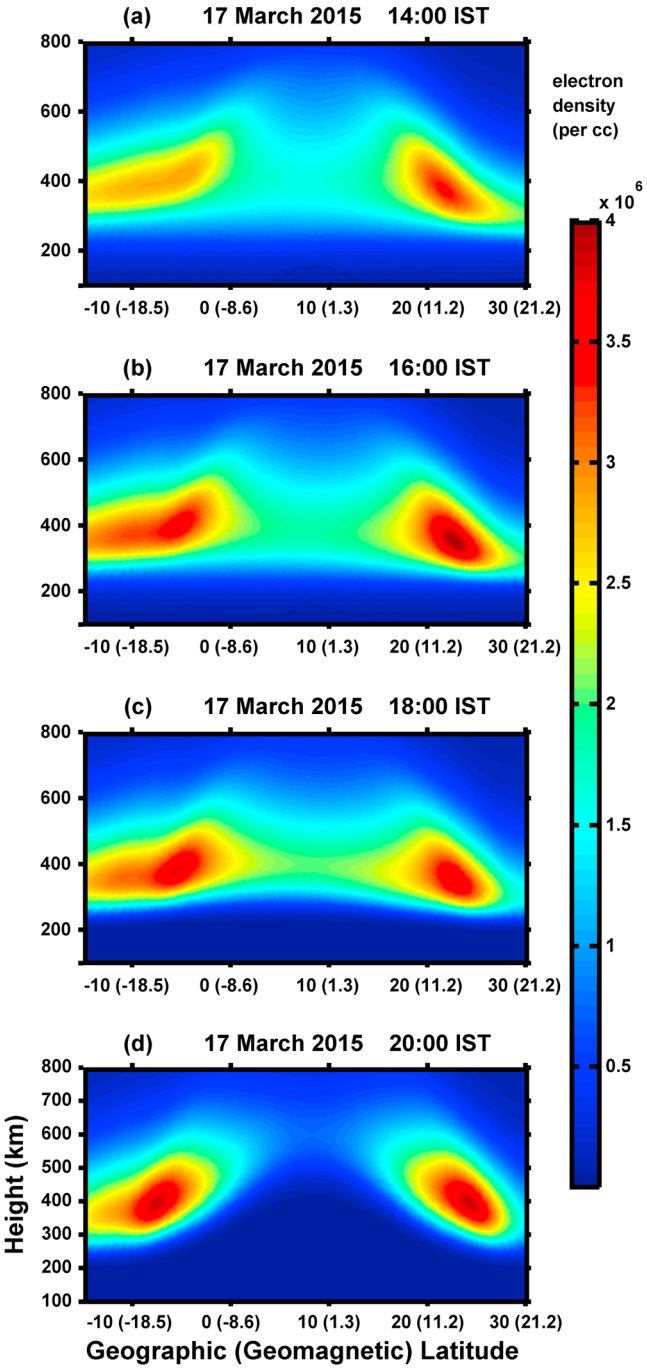

Figure 7. Latitudinal-altitudinal distribution of the ionospheric plasma over Indian longitude in the SAMI2 model on 17 March 2015 at (a) 14 IST, (b) 16 IST, (c) 18 IST, and (d) 20 IST.

that the role of the equatorward neutral wind in the formation of the EIA is secondary in comparison to the eastward electric field.

3.6. Comparison of Model Results With GPS TEC Observations

Total electron content over the Indian longitude during the 16–18 March 2015 is being discussed next. Figure 9 shows the vertical TEC map over Indian longitude derived based on SAMI2 model and six station dual frequency GPS receiver network. Vertical TEC (VTEC) has been derived from the SAMI2 model by integrating the electron density in a vertical column of unit area from 100 km to 1500 km altitude. TEC measured using a network of GPS receivers at six different stations, Tirunelveli (0.4°N magnetic latitude), Bangalore (3.6°N magnetic latitude), Hyderabad (8.5°N magnetic latitude), Nagpur (12.3°N magnetic latitude), Rajkot (14.2°N magnetic latitude), and Lucknow (17.3°N magnetic latitude) in India, have also been used to derive the VTEC map over the Indian region. VTEC map has been constructed by considering the ionospheric pierce point (IPP) to be at 350 km altitude and PRNs with elevation higher than 30° have only been considered. VTEC map has been constructed with a time resolution of 15 min. Unlike for the model, where VTEC map has been derived by the vertical integration of the ionospheric densities, GPS VTEC map has been derived by measuring the slant TEC and converting it to the VTEC over a region where the line of sight intersects the IPP altitude, i.e., 350 km. Figures 9a and 9b present the VTEC variation during 16–18 March 2015 based on SAMI2 model and GPS receiver network, respectively. Both model and observed maps show enhancement in the VTEC during the post sunset period on 17 March in the low latitude. This indicates the enhancement to the EIA due to the activation of the super fountain effect associated with the penetration electric field in the post sunset hours. This enhancement in the TEC over the EIA crest on 17 March, however, is lesser than that reported in previous investigations [eg. *Mannucci et al.*, 2005]. Also, a suppression of the EIA can be seen during the daytime on 18 March, i.e., during the storm recovery phase.

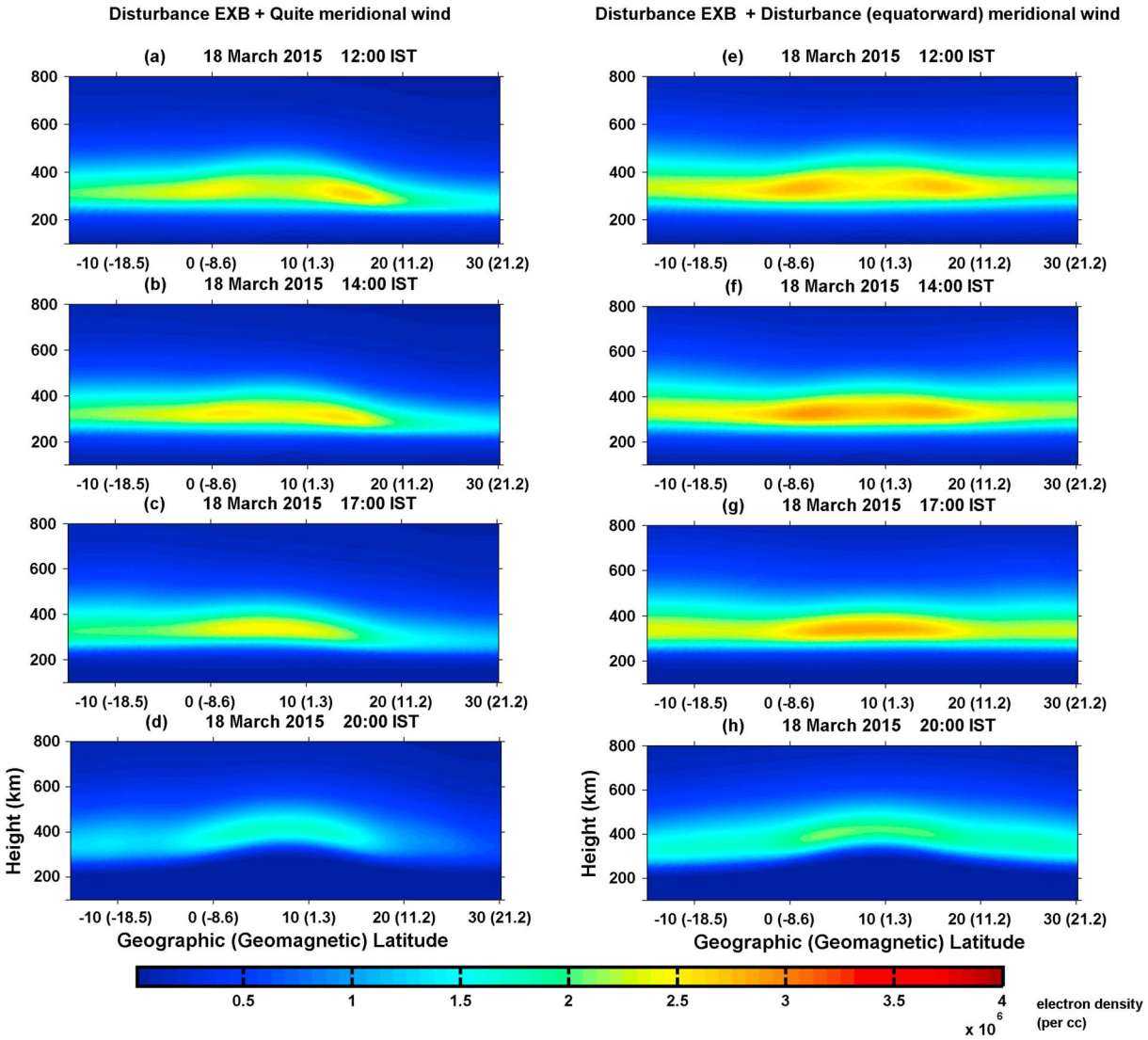

Figure 8. (a–d) Latitudinal-altitudinal distribution of the ionospheric plasma over Indian longitude in the SAMI2 model on 18 March 2015 at 12IST, 14IST, 17IST, and 20IST, respectively, considering the disturbance E × B drift and quiet meridional neutral wind. (e–h) Same as Figures 8a–8d but considering the disturbance E × B drift and disturbance meridional neutral wind.

4. Discussion and Summary

In this paper, modeling investigation of the low-latitude ionospheric response to an intense geomagnetic storm over Indian longitude is being reported. The impact of the geomagnetic storm on the low-latitude ionosphere depends upon the longitude under consideration. The main phase of the geomagnetic storm started in the early post sunset hours over the Indian longitude. This local time is important from the perspective of the prompt penetration of the magnetospheric electric field on to the equatorial region. Vertical E × B drift recorded by the ionosonde at Tirunelveli indicated a very large prereversal enhancement of the zonal electric field. This indicates the effect of the concurrence of prompt penetration electric field and the PRE. The peak h′F recorded by the ionosonde was ~550 km. Investigations in the past have also revealed the role geomagnetic disturbance can play in enormously enhancing the PRE of the zonal field and the post sunset height rise of the *F* layer. *Sobral et al.* [1997], based on the ionosonde observations from Fortaleza, Brazil, during several geomagnetic storms, have reported that the peak h′F during the post sunset hours can exceed the quiet time value by 150–200 km. Also, *Lin et al.* [2005a, 2005b] based on the observational and modeling investigations over American sector have found the prompt penetration electric field to enhance the latitudinal-altitudinal extant of the EIA in the evening hours. Another important aspect

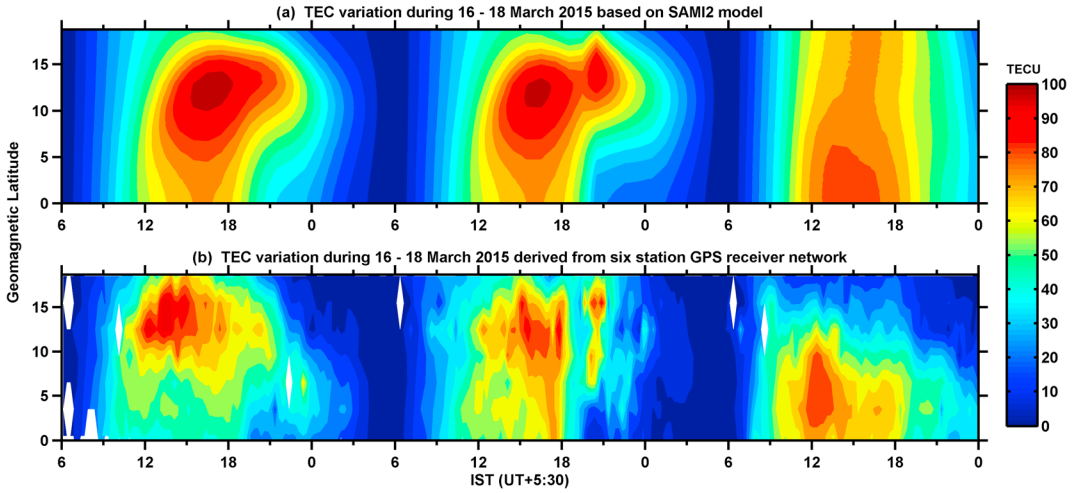

Figure 9. Comparison of the VTEC map derived from SAMI2 model and six station GPS TEC observations. (a) VTEC map derived by integrating the SAMI2 model plasma density in a vertical column of unit area from 100 km to 1500 km. (b) VTEC map derived from GPS observations from six stations in India (refer to the text).

associated with the superstorm is the ionospheric disturbance dynamo. Disturbance dynamo in the recovery phase of the geomagnetic storm has been known to cause suppression of the daytime EIA [*Sastri*, 1988]. In the present investigation also a remarkable suppression of the EIA was seen in the ground-based observation of the TEC (as can be seen in Figure 9b). Coming to the modeling aspects of the present investigation, the SAMI2 model utilizing the intense vertical E × B drift observed during the evening hours on 17 March 2015, indicated a much greater height rise of the *F* layer in comparison with the quiet period. SAMI2 model, incorporating the E × B drift, as indicated in Figure 4c, during the recovery phase of the geomagnetic storm has also indicated a remarkable suppression of the EIA. As mentioned earlier, daytime E × B drift on prestorm, storm, and recovery day has been considered based on Scherliess-Fejer model. Role of the equatorward disturbance wind on the ionospheric plasma density over the equatorial region has also been investigated using the SAMI2 model. Equatorward wind has been found to enhance the plasma density over the equatorial region. However, the formation of the EIA seems to be governed by the polarity of the zonal electric field. Similar results have been earlier reported based on the Sheffield University plasmasphere-ionosphere model by *Balan et al.* [2013], where disturbance meridional wind during the recovery phase has been found to enhance the plasma density in the equatorial ionosphere. They have also found the EIA to be absent when the zonal electric field was assumed to be westward during the daytime.

There were also peculiarities in the model and observational results presented in this investigation vis-a-vis earlier investigations. The enhancement of the TEC in the EIA crest region in the SAMI2 model during the post sunset period on 17 March was significantly less in comparison to earlier investigations on the impact of the prompt penetration electric field on the low-latitude ionosphere. *Mannucci et al.* [2005] have reported a global enhancement in the TEC, in response to interplanetary event, of the order of 40 to 250%. In the present investigation, TEC enhancement in the EIA crest (in model and observation, as indicated in Figure 9) due to the impact of the prompt penetration electric field was of the order of 20–30%, with reference to the quiet period. However, the investigation of *Mannucci et al.* [2005] corresponded to a much more intense space weather event, known as the "Halloween storm," than the one considered in this investigation. Also, their investigation was based on the dayside TEC enhancement due to the prompt penetration of electric field. Modeling investigations in past have also indicated a much intense expansion of the EIA crest latitude and the height rise of the *F* layer, during the prompt penetration of electric field in the evening hours [*Lu et al.*, 2013; *Lin et al.*, 2005b], than that indicated in the present investigation. However, the enhancement in the E × B drift due to the prompt penetration of electric field, considered in those investigations was of the order of 100–150 m/s above the quiet period E × B drift. On the other hand, in the present investigation, the enhancement in the E × B drift due to the prompt penetration electric field was ~40–50 m/s above the quiet period value (as measured by the ionosonde, shown in Figure 2). This difference, partly, is due to the difference in the intensity of the space weather events under consideration. Earlier investigations were carried out on

much more intense interplanetary event than the one considered for this investigation. Also, earlier investigations have focused on the South American sector, where due to lesser geomagnetic field (total magnetic field over Tirunelveli, India, is ~1.6 times more than that over Jicamarca, Peru), the E × B drift enhancement due to same prompt penetration electric field will be much higher than that in the Indian sector. Thus, the intensification of the EIA in terms of crest density and crest latitudinal expansion due to the prompt penetration electric field can be expected to be more remarkable in the American sector than in the Indian sector.

The TEC in the SAMI2 model (Figure 9) prior to the PRE period on 17 March shows a decrease in comparison to the quiet day (due to the short-term effect of ionospheric disturbance dynamo as well as overshielding electric field). This decrease in TEC prior to PRE hours could have possibly influenced the EIA crest density after the PRE hours. However, the drop in the TEC before PRE hours cannot be the primary cause of lesser (than expected) EIA crest after the PRE hours (considering the penetration of electric field during the PRE hours). The difference in the prompt penetration E × B drift magnitude observed in this investigation and in previous reports from South American sector is too large. Thus, the lesser (than expected) EIA crest density post PRE is mainly due to the lesser (than expected) prompt penetration E × B drift (during the PRE hours). Possible reasons for lesser prompt penetration E × B drift have already been discussed in the previous paragraph.

The main points discussed in this paper can be briefly summarized as follows. Due to the concurrence of the prompt penetration of magnetospheric electric field and PRE of zonal equatorial electric field, the peak *F* region vertical E × B drift was recorded ~60–70 m/s in the post sunset hours on 17 March 2015, which is significantly larger than the quiet period value. For plasma density modeling using SAMI2 code, E × B drift during 18–21 IST was considered based on ionosonde observations (on prestorm, storm, and recovery day), while the E × B drift during the remaining hours was considered based on SF model. SAMI2 model indicated a significantly higher post sunset height rise of *F* layer on 17 March (storm day) than on 16 March (quiet day). SAMI2 model also indicated an enhancement in the EIA crest density in the post sunset hours due to the activation of the plasma fountain as a result of the prompt penetration of the electric field. Model also reproduced a suppression of the EIA during the recovery phase of the intense storm, which was found to be consistent with the ground observation of the TEC. Results presented here have also been discussed in the light of earlier investigations on superstorm impact on low-latitude ionosphere. An effort has been made to simulate the features of the low-latitude ionospheric response over the Indian longitude to an intense geomagnetic storm using a combination of model and ionosonde E × B drift.

Acknowledgments

One of the authors (L.M.J.) is thankful to Indian Institute of Geomagnetism Mumbai for providing Nanabhoy Moos Research Fellowship (postdoctoral fellowship) to support the research reported in this manuscript. Authors are also thankful to the technical staff of EGRL in Tirunelveli for operating the CADI. CADI ionosonde data used in this manuscript can be obtained by contacting S. Sripathi or L. M. Joshi (lmjoshi-narl@gmail.com). This work uses the SAMI2 ionosphere model written and developed by the Naval Research Laboratory. SAMI2 code has been modified to incorporate the measured E × B drift. SAMI2 codes are available at NRL website (http://www.nrl.navy.mil/ppd/branches/6790/sami2). Authors would like to thank Prof. D S Ramesh, Director IIG, for his kind support and encouragement to ionospheric modeling studies at IIG. One of the authors (SS) also would like to thank Prof. A Bhattacharyya for her encouragement in this regard.

References

Abdu, M. A., P. T. Jayachandran, J. MacDougall, J. F. Cecile, and J. H. A. Sobral (1998), Equatorial *F* region zonal plasma irregularity drifts under magnetic disturbances, *Geophys. Res. Lett.*, *25*(22), 4137–4140, doi:10.1029/1998GL900117.

Abdu, M. A., J. R. de Souza, J. H. A. Sobral, and I. S. Batista (2006), Magnetic storm associates disturbance dynamo effects over low and equatorial latitude ionosphere, in *Recurrent Magnetic Storms: Corotating Solar Wind Streams*, *Geophysical Monograph Series*, vol. 167, edited by B. Tsurutani et al., pp. 283–304, AGU, Washington, D. C., doi:10.1029/167GM22.

Abdu, M. A., I. S. Batista, F. Bertoni, B. W. Reinisch, E. A. Kherani, and J. H. A. Sobral (2012), Equatorial ionosphere responses to two magnetic storms of moderate intensity from conjugate point observations in Brazil, *J. Geophys. Res.*, *117*, A05321, doi:10.1029/2011JA017174.

Astafyeva, E. (2009), Effects of strong IMF B_z southward events on the equatorial and mid-latitude ionosphere, *Ann. Geophys.*, *27*, 1175–1187, doi:10.5194/angeo-27-1175-2009.

Balan, N., Y. Otsuka, M. Nishioka, J. Y. Liu, and G. J. Bailey (2013), Physical mechanisms of the ionospheric storms at equatorial and higher latitudes during the recovery phase of geomagnetic storms, *J. Geophys. Res. Space Physics*, *118*, 2660–2669, doi:10.1002/jgra.50275.

Batista, I. S., E. R. de Paula, M. A. Abdu, N. B. Trivedi, and M. E. Greenspan (1991), Ionospheric effects of the March 13, 1989, magnetic storm at low and equatorial latitudes, *J. Geophys. Res.*, *96*(A8), 13,943–13,952, doi:10.1029/91JA01263.

Bertoni, F., I. S. Batista, M. A. Abdu, B. W. Reinisch, and E. A. Kherani (2006), A comparison of ionospheric vertical drift velocities measured by Digisonde and incoherent scatter radar at the magnetic equator, *J. Atmos. Sol. Terr. Phys.*, *68*(6), 669–678, doi:10.1016/j.jastp.2006.01.002.

Bibl, K., and B. W. Reinisch (1978), The universal digital ionosonde, *Radio Sci.*, *13*(3), 519–530, doi:10.1029/RS013i003p00519.

Blanc, M., and A. D. Richmond (1980), The ionospheric disturbance dynamo, *J. Geophys. Res.*, *85*, 1669–1686, doi:10.1029/JA085iA04p01669.

Cannon, P. S., B. W. Reinisch, J. Buchau, and T. W. Bullett (1991), Response of the polar cap *F* region convection direction to changes in the interplanetary magnetic field: Digisonde measurements in northern Greenland, *J. Geophys. Res.* *96*(A2), 1239–1250, doi:10.1029/90JA02128.

Carter, B. A., et al. (2014), Using solar wind data to predict daily GPS scintillation occurrence in the African and Asian low-latitude regions, *Geophys. Res. Lett.*, *41*, 8176–8184, doi:10.1002/2014GL062203.

Fejer, B. G. (1997), The electrodynamics of the low-latitude ionosphere: Recent results and future challenges, *J. Atmos. Sol. Terr. Phys.*, *59*, 1465–1482, doi:10.1016/S1364-6826(96)00149-6.

Fejer, B. G. (2002), Low latitude storm time electrodynamics, *J. Atmos. Sol. Terr. Phys.*, *64*, 1401–1408, doi:10.1016/S1364-6826(02)00103-7.

Fejer, B. G., and L. Scherliess (1997), Empirical models of storm time equatorial electric fields, *J. Geophys. Res.*, *102*, 24,047–24,056, doi:10.1029/97JA02164.

Fejer, B. G., M. F. Larsen, and D. T. Farley (1983), Equatorial disturbance dynamo electric fields, *Geophys. Res. Lett.*, *10*, 537–540, doi:10.1029/GL010i007p00537.

Fejer, B. G., J. W. Jensen, T. Kikuchi, M. A. Abdu, and J. L. Chau (2007), Equatorial ionospheric electric fields during the November 2004 magnetic storm, *J. Geophys. Res.*, *112*, A10304, doi:10.1029/2007JA012376.

Fesen, C. G., G. Crowley, and R. G. Roble (1989), Ionospheric effects at low latitudes during the March 22, 1979, geomagnetic storm, *J. Geophys. Res.*, *94*(A5), 5405–5417, doi:10.1029/JA094iA05p05405.

Foster, J. C., and W. Rideout (2005), Mid-latitude TEC enhancements during the October 2003 superstorm, *Geophys. Res. Lett.*, *32*, L12S04, doi:10.1029/2004GL021719.

Galav, P., S. Sharma, and R. Pandey (2011), Study of simultaneous penetration of electric fields and variation of total electron content in the day and night sectors during the geomagnetic storm of 23 May 2002, *J. Geophys. Res.*, *116*, A12324, doi:10.1029/2011JA017002.

Galav, P., S. S. Rao, S. Sharma, G. Gordiyenko, and R. Pandey (2014), Ionospheric response to the geomagnetic storm of 15 May 2005 over midlatitudes in the day and night sectors simultaneously, *J. Geophys. Res. Space Physics*, *119*, 5020–5031, doi:10.1002/2013JA019679.

Gonzales, C. A., M. C. Kelley, B. G. Fejer, J. F. Vickrey, and R. F. Woodman (1979), Equatorial electric fields during magnetically disturbed conditions: 2. Implications of simultaneous auroral and equatorial measurements, *J. Geophys. Res.*, *84*, 5803–5812, doi:10.1029/JA084iA10p05803.

Grant, I. F., J. W. MacDougall, J. M. Ruohoniemi, W. A. Bristow, G. J. Sofko, J. A. Koehler, D. Danskin, and D. André (1995), Comparison of plasma flow velocities determined by the ionosonde Doppler drift technique, SuperDARN radars, and patch motion, *Radio Sci.*, *30*(5), 1537–1549, doi:10.1029/95RS00831.

Haaser, R. A., R. Davidson, R. A. Heelis, G. D. Earle, S. Venkatraman, and J. Klenzing (2013), Storm time meridional wind perturbations in the equatorial upper thermosphere, *J. Geophys. Res. Space Physics*, *118*, 2756–2764, doi:10.1002/jgra.50299.

Ho, C. M., A. J. Mannucci, L. Sparks, X. Pi, U. J. Lindqwister, B. D. Wilson, B. A. Iijima, and M. J. Reyes (1998), Ionospheric total electron content perturbations monitored by the GPS global network during two Northern Hemisphere winter storms, *J. Geophys. Res.*, *103*, 26,409–26,420, doi:10.1029/98JA01237.

Huba, J. D., G. Joyce, and J. A. Fedder (2000), Sami2 is Another Model of the Ionosphere (SAMI2): A new low-latitude ionosphere model, *J. Geophys. Res.*, *105*(A10), 23,035–23,053, doi:10.1029/2000JA000035.

Jakowski, N., S. Schulter, and E. Sardon (1999), Total electron content of the ionosphere during the geomagnetic storm on 10 January 1997, *J. Atmos. Sol. Terr. Phys.*, *61*, 299–307, doi:10.1016/S1364-6826(98)00130-8.

Joshi, L. M., S. Balwada, T. K. Pant, and S. G. Sumod (2015), Investigation on *F* layer height rise and equatorial spread *F* onset time: Signature of standing large-scale wave, *Space Weather*, *13*, doi:10.1002/2014SW001129.

Kelley, M. C., B. G. Fejer, and C. A. Gonzales (1979), An explanation for anomalous ionospheric electric fields associated with a northward turning of the interplanetary magnetic field, *Geophys. Res. Lett.*, *6*, 301–304, doi:10.1029/GL006i004p00301.

Kikuchi, T., H. Luhr, T. Kitamura, O. Saka, and K. Schlegel (1996), Direct penetration of the polar electric field to the equator during a*DP*2 event as detected by the auroral and equatorial magnetometer chains and the EISCAT radar, *J. Geophys. Res.*, *101*, 17,161–17,173, doi:10.1029/96JA01299.

Kikuchi, T., H. Liihr, K. Schlegel, H. Tachihara, M. Shinohara, and T.-I. Kitamura (2000), Penetration of auroral electric fields to the equator during a substorm, *J. Geophys. Res.*, *105*(A10), 23,251–23,261, doi:10.1029/2000JA900016.

Lin, C. H., A. D. Richmond, J. Y. Liu, H. C. Yeh, L. J. Paxton, G. Lu, H. F. Tsai, and S.-Y. Su (2005a), Large-scale variations of the low-latitude ionosphere during the October–November 2003 superstorm: Observational results, *J. Geophys. Res.*, *110*, A09S28, doi:10.1029/2004JA010900.

Lin, C. H., A. D. Richmond, R. A. Heelis, G. J. Bailey, G. Lu, J. Y. Liu, H. C. Yeh, and S.-Y. Su (2005b), Theoretical study of the low- and midlatitude ionospheric electron density enhancement during the October 2003 superstorm: Relative importance of the neutral wind and the electric field, *J. Geophys. Res.*, *110*, A12312, doi:10.1029/2005JA011304.

Lin, C. H., A. D. Richmond, J. Y. Liu, G. J. Bailey, and B. W. Reinisch (2009), Theoretical study of new plasma structures in the low-latitude ionosphere during a major magnetic storm, *J. Geophys. Res.*, *114*, A05303, doi:10.1029/2008JA013951.

Lu, G., J. D. Huba, and C. Valladares (2013), Modeling ionospheric super-fountain effect based on the coupled TIMEGCM-SAMI3, *J. Geophys. Res. Space Physics*, *118*, 2527–2535, doi:10.1002/jgra.50256.

Mannucci, A. J., B. T. Tsurutani, B. A. Iijima, A. Komjathy, A. Saito, W. D. Gonzalez, F. L. Guarnieri, J. U. Kozyra, and R. Skoug (2005), Dayside global ionospheric response to the major interplanetary events of October 29–30, 2003 "Halloween storms", *Geophys. Res. Lett.*, *32*, L12S02, doi:10.1029/2004GL021467.

Maruyama, T., G. Ma, and M. Nakamura (2004), Signature of TEC storm on 6 November 2001 derived from dense GPS receiver network and ionosonde chain over Japan, *J. Geophys. Res.*, *109*, A10302, doi:10.1029/2004JA010451.

Rastogi, R. G., and J. A. Klobuchar (1990), Ionospheric electron content within the equatorial anomaly belt, *J. Geophys. Res.*, *95*, 19,045–19,052, doi:10.1029/JA095iA11p19045.

Richmond, A. D., C. Peymirta, and R. G. Roble (2003), Long-lasting disturbances in the equatorial ionospheric electric field simulated with a coupled magnetosphere-ionosphere-thermosphere model, *J. Geophys. Res.*, *108*(A3), 1118, doi:10.1029/2002JA009758.

Sastri, J. H. (1988), Equatorial electric fields of ionospheric disturbance dynamo origin, *Ann. Geophys.*, *6*, 635–642.

Scherliess, L., and B. Fejer (1997), Storm time dependence of equatorial disturbance dynamo zonal electric fields, *J. Geophys. Res.*, *102*, 24,037–24,046, doi:10.1029/97JA02165.

Scherliess, L., and B. G. Fejer (1999), Radar and satellite global equatorial *F* region vertical drift model, *J. Geophys. Res.*, *104*(A4), 6829–6842, doi:10.1029/1999JA900025.

Sharma, S., P. Galav, N. Dashora, S. Alex, R. S. Dabas, and R. Pandey (2011), Response of low-latitude ionospheric total electron content to the geomagnetic storm of 24 August 2005, *J. Geophys. Res.*, *116*, A05317, doi:10.1029/2010JA016368.

Singh, R., S. Sripathi, S. Sreekumar, S. Banola, K. Emperumal, P. Tiwari, and B. S. Kumar (2015), Low-latitude ionosphere response to super geomagnetic storm of 17/18 March 2015: Results from a chain of ground-based observations over Indian sector, *J. Geophys. Res. Space Physics*, *120*, 10,864–10,882, doi:10.1002/2015JA021509.

Sobral, J. H. A., M. A. Abdu, W. D. González, B. T. Tsurutani, I. S. Batista, and A. L. C. deGonzález (1997), Effects of intense storms and substorms on the equatorial ionosphere/thermosphere system in the American sector from ground-based and satellite data, *J. Geophys. Res.*, *102*(A7), 14,305–14,313, doi:10.1029/97JA00576.

Tsurutani, B., et al. (2004), Global dayside ionospheric uplift and enhancement associated with interplanetary electric field, *J. Geophys. Res.*, *109*, A08302, doi:10.1029/2003JA010342.

Tsurutani, B. T., et al. (2008), Prompt penetration electric fields (PPEFs) and their ionospheric effects during the great magnetic storm of 30–31 October 2003, *J. Geophys. Res.*, *113*, A05311, doi:10.1029/2007JA012879.

Woodman, R. F., J. L. Chau, and R. R. Ilma (2006), Comparison of ionosonde and incoherent scatter drift measurements at the magnetic equator, *Geophys. Res. Lett.*, *33*, L01103, doi:10.1029/2005GL023692.